JOURNAL OF AIRCRAFT
Vol. 34, No. 4, July–August 1997

Sideslip Behavior of Elliptic Cross-Sectional Forebodies at High Angle of Attack

Amir H. Tajfar* and Peter J. Lamont†
University of Manchester, Manchester M13 9PL, England, United Kingdom

This paper reports on the results of tests conducted on two elliptical cross-sectional forebodies with major/minor axis ratios of 1:0.8 and 1:0.6, respectively. The experiments were performed in a Reynolds number range between 8×10^4 and 3.1×10^5 (based on major axis of the ellipse). These elliptical forebodies were found to have unique sideslip behavior in contrast to the multiple solutions that have been found for circular cross-sectional forebodies. When the major axis of the elliptic forebody is in line with the aircraft *y*-body axis (termed flat ellipse) the forebody is directionally stable. When the major axis of the ellipse is in line with the aircraft *z*-body axis (termed vertical ellipse) the forebody is directionally unstable. The effect of turbulent reattachment on one side of the body is described. It was found that reattachment increases the directional instability of vertical ellipses.

Nomenclature

C_N = normal force coefficient, $\frac{1}{2}\rho v^2 S$
C_{NA} = normal force coefficient, total incidence plane
C_n = yawing moment coefficient, $\frac{1}{2}\rho v^2 SL$
$C_{n\beta}$ = $dC_n/d\beta$
C_P = pressure coefficient
C_y = side force coefficient, $\frac{1}{2}\rho v^2 S$
C_{yA} = side force coefficient, total incidence plane
h = axis of ellipse in pitch plane
L = length of the body
Re = Reynolds number based on major axis of the ellipse
S = maximum cross-sectional area
v = freestream velocity
w = axis of ellipse in the sideslip plane
x, y, z = body axes
α = angle of attack
β = sideslip angle
ρ = density
σ = total incidence angle, $\cos^{-1}(\cos\alpha \cos\beta)$
ϕ = effective roll angle, $\tan^{-1}(\tan\beta/\sin\alpha)$

Introduction

HIGH-performance combat aircraft fly at very high angles of attack to obtain the turning performance required to maneuver effectively. At such high angles of attack, fighter configurations can experience large aerodynamic asymmetries along with severe degradation in lateral stability. This can result in loss of control and possible spin entry. Experiments on aircraft models with circular cross-sectional (CCS) forebodies indicate the presence of strong yawing moments at high angles of attack.[1] The yawing moment produced by sharp-nosed forebodies can exceed the moment produced by full rudder deflection, even at relatively low angles of attack. In addition, rudder effectiveness decreases significantly as the angle of attack increases.

This situation alone poses severe problems to aircraft designers. However, there is an even more serious problem associated with CCS forebodies. Their sideslip behavior at high angle of attack can be very nonlinear and, in particular, different sideslip behaviors have been reported on identical-shaped bodies.[2,3] Lamont and Kennaugh[4,5] explained why multiple solutions occur for CCS forebodies. They used the geometric transformation between aircraft body axes and the total incidence plane to explain how the unpredictability of the variation of side force with roll angle leads to a variety of sideslip behaviors for all CCS forebodies at high incidence. Because the roll signature of CCS forebodies depends on minute geometric variations at the nose tip, it is impossible to predict the sideslip behavior of any particular aircraft with a CCS forebody at high angle of attack.

Aircraft designers have looked for alternative forebody shapes. The most popular alternative cross-sectional shape is an elliptic cross section (ECS).[6,7] These forebodies are either in the form of a flat ellipse (with the major axis of elliptic forebody in line with aircraft y axis) or a vertical ellipse (with the major axis of the elliptic forebody in line with aircraft z axis).

This paper reports on an experimental investigation into the aerodynamic forces and moments acting on aircraft forebodies with elliptic cross-sectional shapes at high angles of attack. The sideslip behavior of both flat and vertical ellipses has been investigated by using direct sideslip tests and by using roll signature results and the principle of the total incidence plane. The effects of changing Reynolds number on the forces acting on the body have also been investigated.

Forces Acting on a Body at Sideslip

Figure 1 illustrates a forebody at a combined angle of attack and sideslip. The aerodynamic forces acting on the body, in and perpendicular to the total incidence plane (which contains the freestream velocity vector and body x axis), as well as those in the conventional body axis are shown in Fig. 1. The force components referred to body axes can be obtained from those in the total incidence plane as follows:

$$C_N = C_{NA}\cos\phi + C_{yA}\sin\phi \tag{1}$$

$$C_y = C_{yA}\cos\phi - C_{NA}\sin\phi \tag{2}$$

Testing a body at a combined angle of attack and sideslip is equivalent to testing the same body at equivalent effective total incidence and roll angle. The effective total incidence and roll

Received Oct. 5, 1995; revision received March 4, 1997; accepted for publication March 5, 1997.

*Engineer, Department of Aerospace Engineering.
†Lecturer, Department of Aerospace Engineering. Senior Member AIAA.

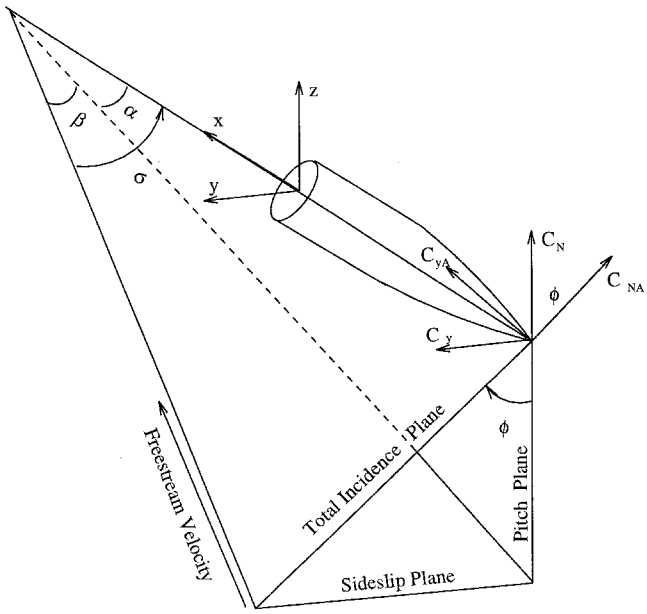

Fig. 1 Aerodynamic force component acting on a body in and perpendicular to the total incidence plane, and in conventional body axis.

angle may be obtained from sideslip angle and the angle of attack in the pitch plane as follows:

$$\cos \sigma = \cos \alpha * \cos \beta \tag{3}$$

$$\tan \phi = \tan \beta / \sin \alpha \tag{4}$$

The implication is that sideslip results can simply be obtained from zero sideslip tests, where only roll angle and incidence are changed. Therefore, in this paper the sideslip results were investigated by using both direct sideslip tests and roll signature results.

Experimental Details

The experiments were conducted in a (1.1 × 0.87 m) subsonic wind tunnel at the Goldstein Research Laboratory of the University of Manchester. The turbulence level of the tunnel was about 0.65%. The forces and moments were measured by using the six-component balance system of the tunnel. The support system is illustrated in Fig. 2. The support system was designed to cause minimum interference with the flow around the model. The sting was long enough to provide adequate clearance between the model and the main strut. The positive angle of attack was measured downward, hence there was more clearance between the model and strut at higher angles of attack. The model can be pitched and yawed without any adjustment to the support system. But roll angle had to be changed manually, i.e., the tunnel had to be stopped and roll angle be changed and adjusted manually. Three forebodies were tested, two with elliptical cross sections (with major/minor axis ratios of 1:0.8 and 1:0.6, respectively) and one with circular cross section. All forebodies had a nose fineness ratio of 3, i.e., nose length to the maximum minor axis length for ECS forebodies and nose length to the maximum diameter for CCS forebody. The lengths of afterbodies were three times the minor axis length for the ECS forebodies and three times the diameter for the CCS forebody. The roll signature results were obtained by positioning the model at the reference zero roll attitude and testing it through a 20- to 90-deg incidence range. The process was repeated through 0- to 360-deg roll orientations at every 15-deg roll interval (5-deg interval near side force switch). The sideslip tests were performed by positioning the model at an angle of attack and then sideslipping it. Each model had a set of 36 pressure tappings located 3.3 diameters aft of the nose tip. The moments were measured about the base of the model. The maximum error for the force and moment coefficients are ±0.15 and ±0.21, respectively. The accuracy of pressure transducer is 0.5% of the maximum pressure of 7200 Pa. This corresponds to a maximum error of ±0.015 for the pressure coefficient corresponding to the minimum operating speed. Typical range of the repeatability of the experimental data is illustrated in Fig. 3.

Total Incidence Plane Results

Zero Roll Tests

These three models can be used to produce zero sideslip results for five different height-to-width (h/w) ratios. The variations of side force and normal force with angle of attack for different h/w ratio models at zero roll are illustrated in Figs. 3

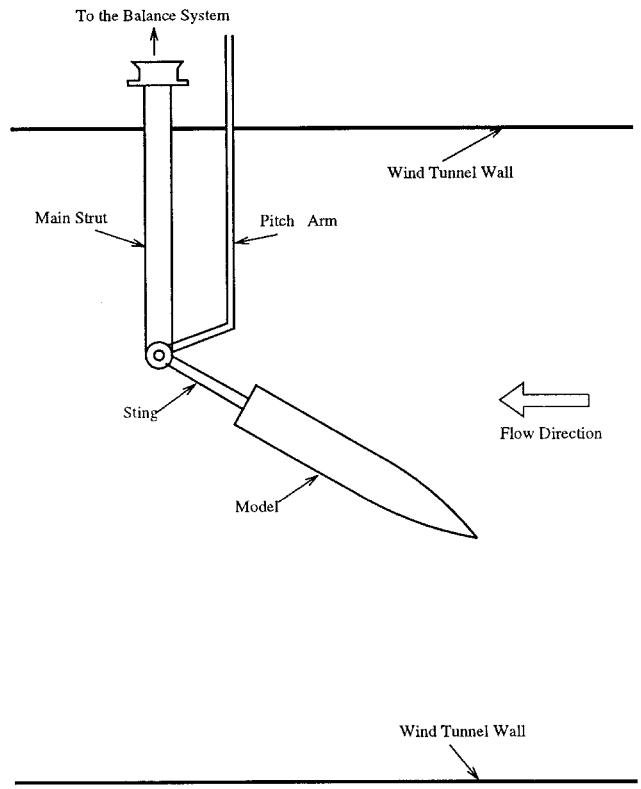

Fig. 2 Support system and the model in the test section of the tunnel.

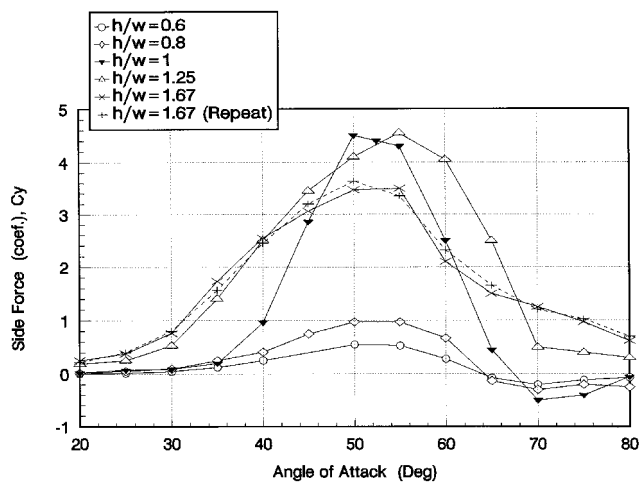

Fig. 3 Side force variations with angle of attack for different h/w ratios.

and 4, respectively. As shown in Fig. 3, reducing h/w from 1.67 to 1 has little effect on the side force, although for a higher h/w, asymmetry starts at a lower angle of attack. Further reduction in h/w below 1 results in a significant drop in asymmetry. The normal force results in Fig. 4 indicate that reducing h/w from 1.67 to 1 causes a significant increase in normal force. Further reduction in h/w below 1 results in a further small increase in the normal force.

The preceding results indicate that reducing h/w below 1 (flat ellipses) causes a significant reduction in asymmetry and a small increase in normal force. On the other hand, increasing h/w above 1 (vertical ellipses) results in a significant reduction in normal force and a small increase in asymmetry.

Roll Signature Results

This section concentrates on the roll signature results, i.e., the results at different angles of attack for various roll orientations, and in particular, changes in the direction of side force as roll orientation is changed. The experimental results for each elliptical model were obtained by rolling the model through 360 deg. The zero roll datum corresponds to a flat ellipse at zero roll and 90 deg corresponds to a vertical ellipse at zero roll. The results from the two elliptical models are similar. The roll-angle variations are illustrated in Fig. 5, taking results from the 1:0.6 elliptical model. Roll signature results for 0- to 180-deg roll angle range are virtually identical to 180- to 360-deg roll angle range. The side force variation with roll angle for the CCS model at 50-deg angle of attack (which corresponds to the maximum side force), is also included in the figure. The change in direction of side force for the CCS model can happen at any roll orientation, depending on the chosen zero roll attitude datum and infinitesimal geometric asymmetries at the nose tip. In contrast, for ECS forebodies, side force changes sign four times in a complete roll signature. The change in direction of side force occurs at known roll orientations, i.e., with both flat and vertical ellipses near zero roll angle. Therefore, unlike CCS forebodies, there is no unexpected change in the direction of side force with roll angle.

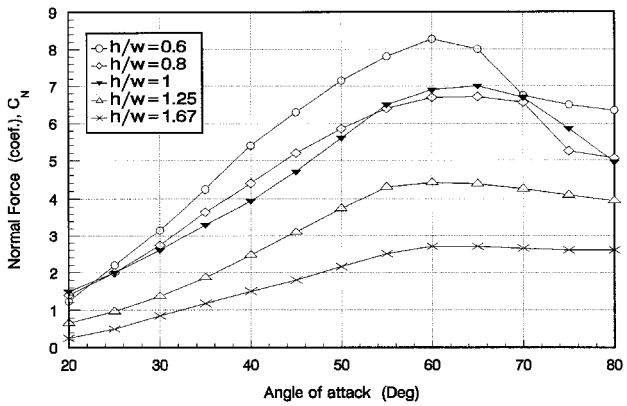

Fig. 4 Normal force variations with angle of attack for different h/w ratios.

For flat ellipses positive roll (starboard wing down) causes positive side force and negative roll causes negative side force. The opposite is true for vertical ellipses where positive roll produces negative side force and negative roll produces positive side force.

For both flat and vertical ellipses, the magnitude of the side force increases with roll angle. The rate of change of side force with roll angle for vertical ellipses near zero roll is greater than for flat ellipses near zero roll.

The variations of normal force with roll orientation (for the 1:0.6 model) are illustrated in Fig. 6. Maximum normal force is obtained with the flat ellipse near zero roll. As the flat ellipse is rolled, the normal force drops and reaches a minimum, which corresponds to the vertical ellipse near zero roll.

The previous results indicate that maximum value of side force is obtained between about 45- to 60-deg roll attitudes, i.e., with the vertical ellipse between 30- to 45-deg roll angle. Whereas, maximum normal force is obtained with the flat ellipse near zero roll angle. The side force produced by ECS forebodies is considerably higher than the maximum side force for CCS forebodies, except for flat ellipses near zero roll angle. On the other hand, the normal force for the CCS forebodies is quite high in comparison and is close to the maximum obtainable normal force, i.e., for flat ellipses (see Fig. 4).

Sideslip Results

In this section the sideslip results for flat and vertical ellipses will be examined. The side force sideslip behaviors for the

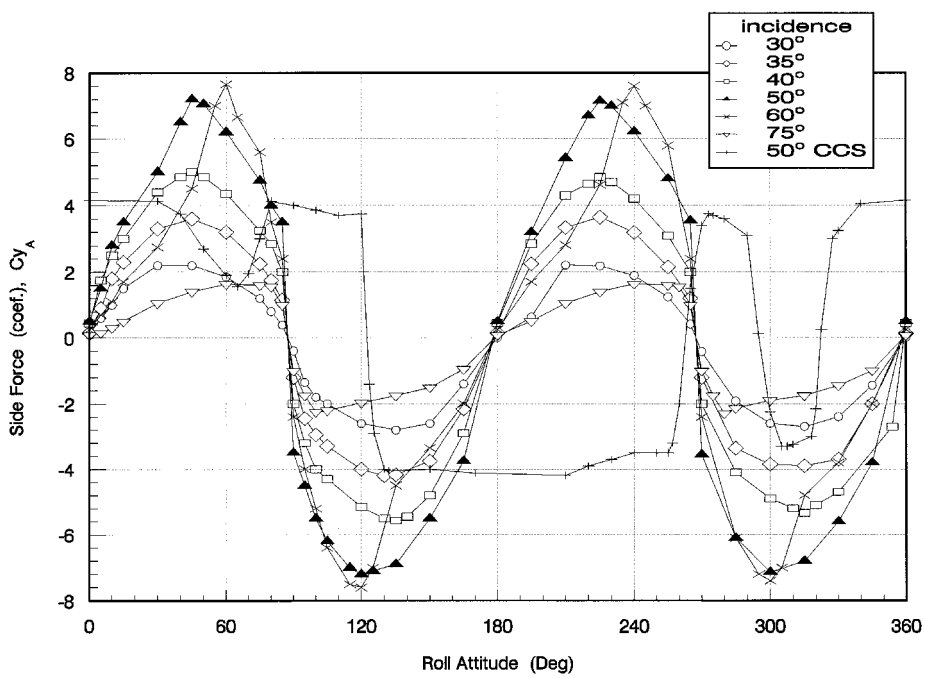

Fig. 5 Side force variations with roll attitude for the 1:0.6 model at $Re = 1.2 \times 10^5$.

1:0.6 flat ellipse are illustrated in Fig. 7. The results indicate that for flat ellipses there is local directional stability near zero sideslip. As angle of attack increases, the local stability region is reduced, but the slope of the curve, in the local stability region, increases. The side force sideslip behaviors for the 1:0.6 vertical ellipse are shown in Fig. 8. As illustrated, side force behavior near zero sideslip leads to instability because side force tends to further increase the sideslip.

The previous results indicate that unlike CCS forebodies, ECS forebodies have unique sideslip behaviors, i.e., flat ellipses are directionally stable and vertical ellipses are directionally unstable. Therefore, their sideslip behaviors are more predictable.

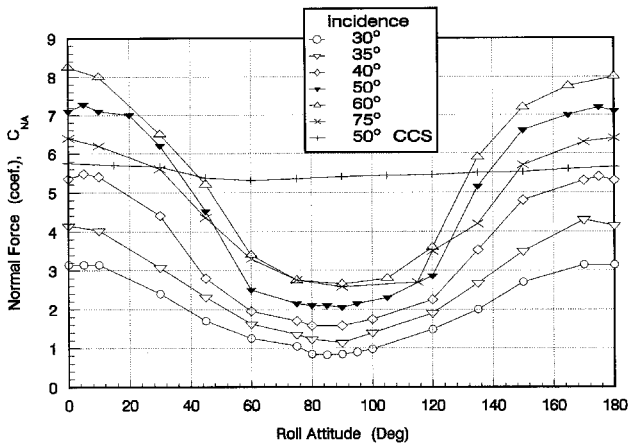

Fig. 6 Normal force variations with roll attitude for the 1:0.6 model at $Re = 1.2 \times 10^5$.

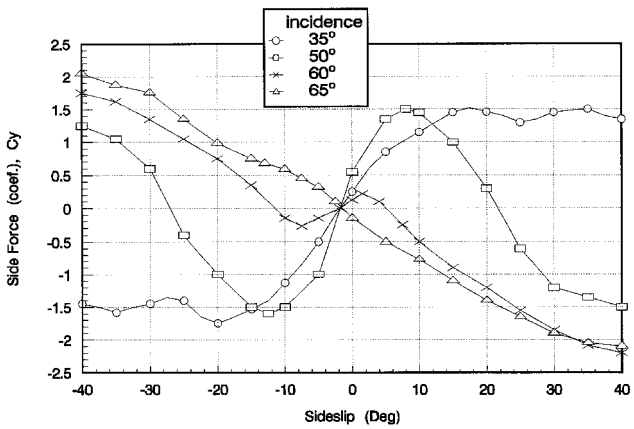

Fig. 7 Side force variations with sideslip for the 1:0.6 flat ellipse at $Re = 1.2 \times 10^5$.

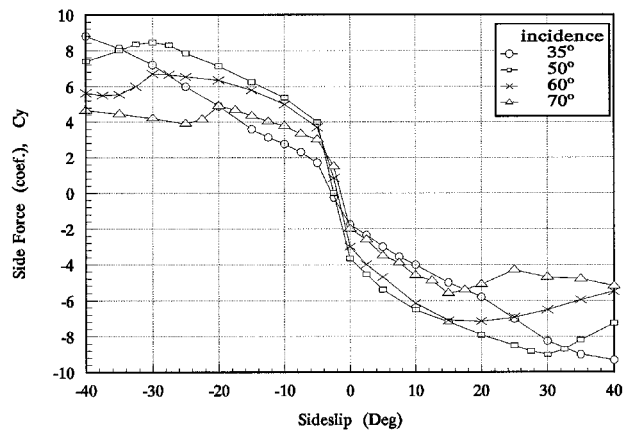

Fig. 8 Side force variations with sideslip for the 1:0.6 vertical ellipse at $Re = 1.2 \times 10^5$.

To better understand the favorable and unfavorable contributions of flat and vertical ellipses to directional stability, respectively, some smoke wire tests were performed. Instead of performing sideslip tests, the forebodies were tested at roll angle. The relationship between sideslip and roll angle is given in Eq. (4).

The smoke wire experiments were performed at a Reynolds number of 3×10^4, which corresponds to laminar separation, similar to the previous force results. The smoke wire photographs were taken from upstream of the model that was the 1:0.8 ellipse at 50-deg incidence. Figures 9 and 10 show the vertical and flat ellipses, respectively, at +5-deg roll, which corresponds to +3.8 deg of sideslip. Separation positions have been superimposed on the photographs to aid the flow analysis. Consider the flow around the vertical ellipse shown in Fig. 9. There is some delay in primary separation on the port side in comparison to the starboard side. The flow accelerates to a higher speed on the port side. This produces a suction force to the port side that tends to increase the sideslip. In the case of the flat ellipse (see Fig. 10), there is less asymmetry between the primary separation lines on the two sides of the body. Suction pressure is higher on the starboard side of body where the vortex is formed closer to the surface than on the port side. Therefore, a side force is produced to the starboard side, which tends to reduce the sideslip.

Insight into the sideslip behavior is best obtained by examining the variation of maximum $C_{n\beta}$ (near zero sideslip) with angle of attack (see Fig. 11). The favorable contribution of flat ellipses and the unfavorable contribution of vertical ellipses to directional stability are clearly visible. The degradation in directional stability for vertical ellipses is more significant than the beneficial contribution for flat ellipses. Increasing major/minor axis ratio reduces both the beneficial

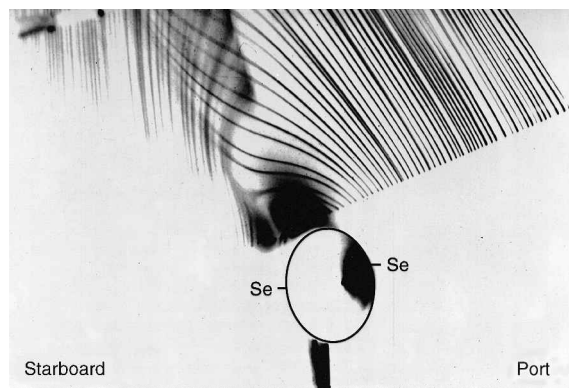

Fig. 9 Smoke wire results for the 1:0.8 vertical ellipse at +5-deg roll and 50-deg angle of attack (view from the front).

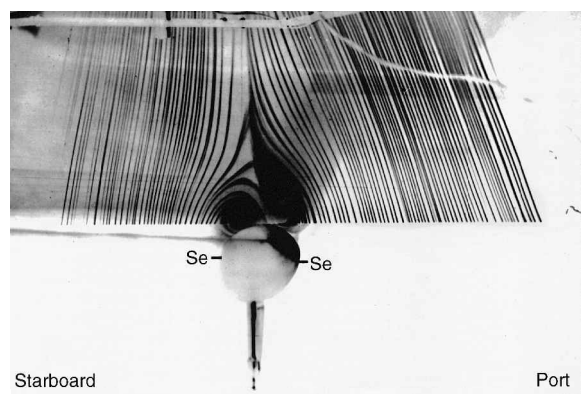

Fig. 10 Smoke wire results for the 1:0.8 flat ellipse at +5-deg roll and 50-deg angle of attack (view from the front).

contribution of flat ellipses to directional stability and the instability of vertical ellipses. The magnitude of $C_{n\beta}$ for both flat and vertical ellipses increases with angle of attack up to about 60 deg. Because of the change in side force with roll angle, $C_{n\beta}$ can have different values for CCS forebodies, depending on the initial roll setting of the nose. The boundaries for $C_{n\beta}$ variations with angle of attack, for the CCS forebody, are included in Fig. 11. In comparison to flat ellipses, CCS forebodies can have a more significant beneficial contribution to directional stability. On the other hand, maximum directional instability of CCS forebodies is less significant compared to that of vertical ellipses.

The principle of total incidence plane can be used to produce sideslip results from roll signature data. An example is shown in Fig. 12 for the 1:0.8 vertical ellipse at 50-deg angle of attack. The solid line in Fig. 12 represents the sideslip results and the points are those calculated from roll signature data. The agreement between two sets of data is excellent, which is a clear indication that the sideslip results could simply be obtained from roll signature data.

Reynolds Number Effects

Turbulent reattachment starts to occur after primary separation (on one side of the body) as the Reynolds number increases beyond a critical value. Reattachment produces some changes in the values of forces and moments. These changes are more evident for the 1:0.6 model in comparison to the 1:0.8 model. Figure 13 illustrates the side force variations with angle of attack for the 1:0.6 vertical ellipse at Reynolds numbers below and above the critical value. The effects of reattachment are a drop in side force up to 55-deg angle of attack followed by a large increase in side force between 55–90 deg. Reynolds number effects at angles of attack greater than 55 deg are alternatively shown in the plot of side force against the Reynolds number (see Fig. 14). As indicated, an increase in Reynolds number beyond the critical value produces a jump in the magnitude of the side force. The increase in side force happens at about the same Reynolds number for the incidence range shown. Turbulent reattachment produces a drop in the value of normal force (see Fig. 15). The drop in normal force becomes more significant as incidence increases.

When the model was set at other roll angles, Reynolds number effects were once again confined to incidences above 55 deg. The increase in side force as Reynolds number exceeds a critical value is evident in Fig. 16. Turbulent reattachment starts to occur at a higher Reynolds number as the angle of attack is increased. Whereas, for the 1:0.6 vertical ellipse (at zero roll) reattachment starts to occur at nearly the same Reynolds number for the 55- to 90-deg incidence range.

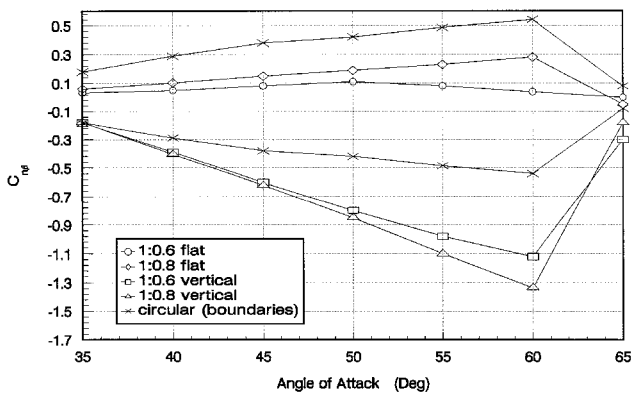

Fig. 11 Variations of $C_{n\beta}$ with angle of attack.

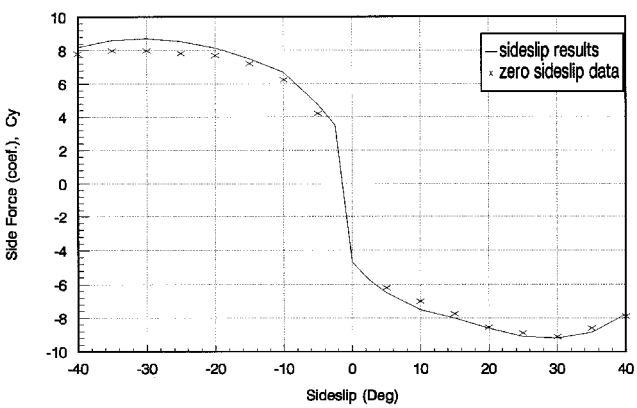

Fig. 12 Sideslip results for the 1:0.8 vertical ellipse at 50-deg angle of attack.

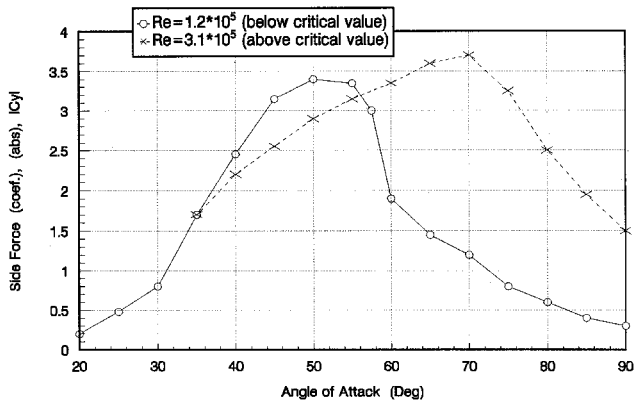

Fig. 13 Side force variations with angle of attack for the 1:0.6 vertical ellipse.

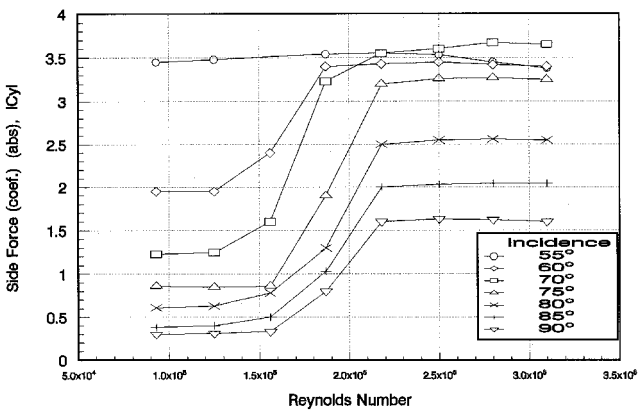

Fig. 14 Side force changes with Reynolds number for the 1:0.6 vertical ellipse.

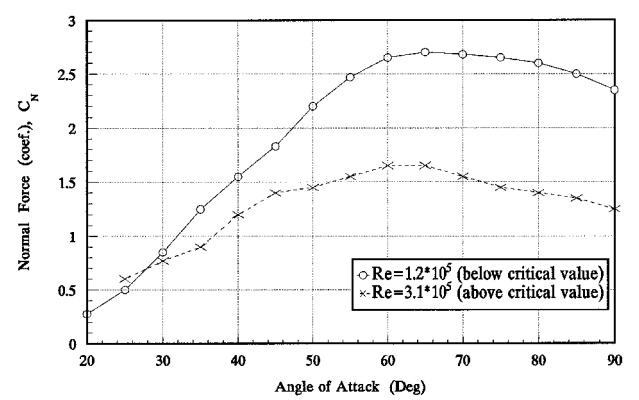

Fig. 15 Normal force variations with angle of attack for the 1:0.6 vertical ellipse.

The occurrence of turbulent reattachment can best be detected by using surface flow visualization. Figure 17 shows the surface flow pattern (viewed from the port side) for the 1:0.6 vertical ellipse at 75-deg angle of attack and 25-deg roll at Reynolds numbers below and above the critical value. The occurrence of reattachment at all stations along the body is clearly visible in Fig. 17b. The changes in the wake flow pattern are shown in Fig. 18. There is little change in the positions of primary separations. At a Reynolds number above the critical value, turbulent reattachment occurs on the port side and separation bubble is formed. The wake size reduces considerably.

An alternative way of observing the changes in the flow around the body, when reattachment occurs, is to take pressure measurements. The pressure results for the previous cases are illustrated in Fig. 19. At a Reynolds number above the critical value, turbulent reattachment occurs on the port side. This results in a significant increase in the suction peak on the port side with a subsequent large increase in the side force. Turbulent flow can better sustain adverse pressure gradient, hence, there is a considerable pressure recovery and some delay in the final separation, which causes an increase in the wake pressure and a reduction in the wake size. These produce a drop in the value of normal force. Side force increases, at a Reynolds number above the critical value, mainly because reattachment only occurs on one side. If turbulent reattachment occurs on both sides, the change in side force, in comparison to laminar separation, becomes less significant (see Fig. 20). Further changes will occur with increasing Reynolds number until the

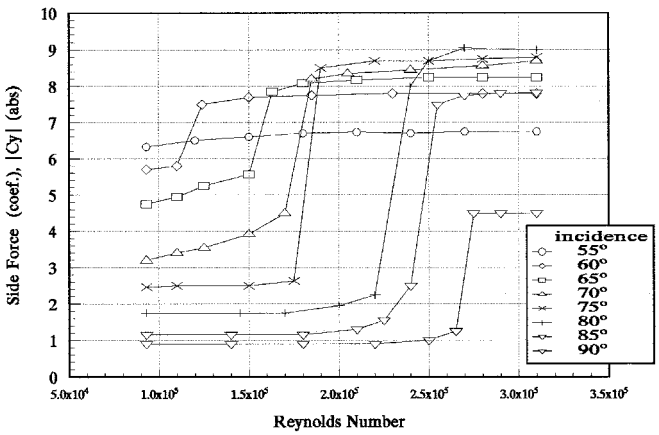

Fig. 16 Side force variations with Reynolds number for the 1:0.6 vertical ellipse at 25-deg roll angle.

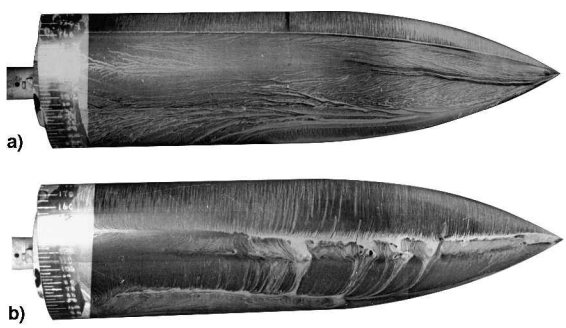

Fig. 17 Surface flow pattern for the 1:0.6 vertical ellipse at 25-deg roll and 75-deg angle of attack (view from the port side) at a Reynolds number a) below and b) above the critical value.

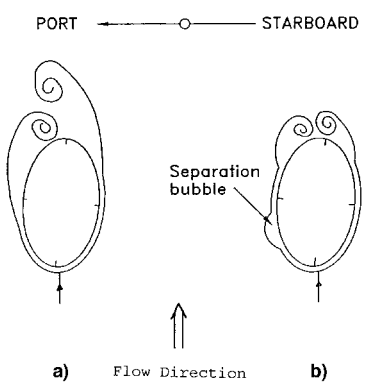

Fig. 18 Two-dimensional crossflow sketches for the 1:0.6 vertical ellipse at 25-deg roll and 75-deg angle of attack (view from downstream) at a Reynolds number a) below and b) above critical value.

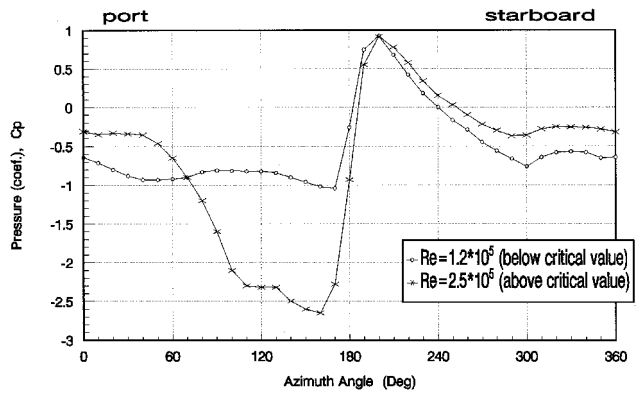

Fig. 19 Effects of Reynolds number on the pressure distribution around the 1:0.6 vertical ellipse at 75-deg angle of attack and 25-deg roll angle.

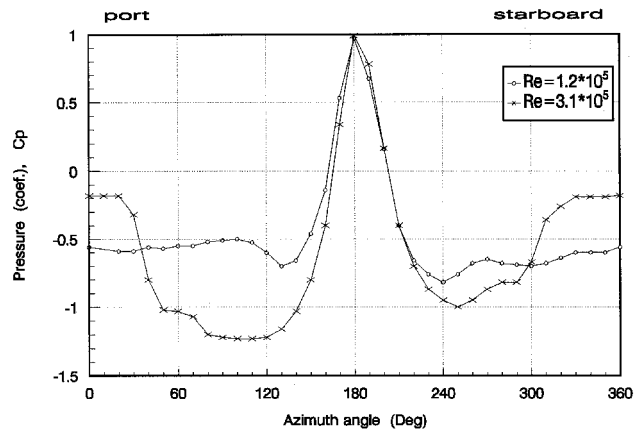

Fig. 20 Effects of Reynolds number on the pressure distribution around the 1:0.6 vertical ellipse at 80-deg angle of attack.

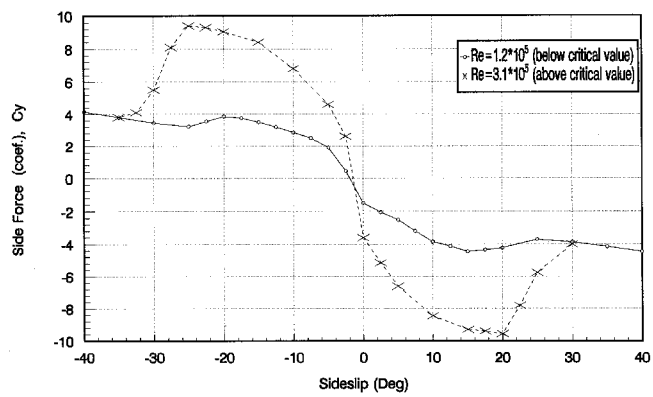

Fig. 21 Side force variations with sideslip for the 1:0.6 vertical ellipse at 70-deg angle of attack.

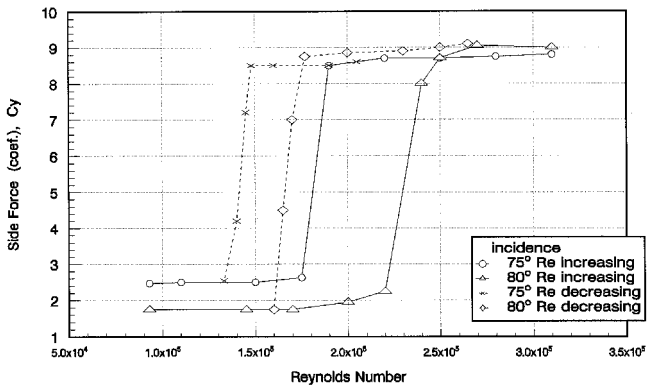

Fig. 22 Hysteresis effects of the side force variations with Reynolds number for the 1:0.6 vertical at −25-deg roll.

situation is reached where primary separation on both sides of the body is turbulent.

The sideslip behaviors for the 1:0.6 vertical ellipse at Reynolds numbers below and above the critical value are illustrated in Fig. 21. Reattachment results in a negative increase in $C_{n\beta}$ and, hence, further degradation in directional stability.

There are some hysteresis effects for the variation of force and moments with Reynolds number near the critical value. This is illustrated in Fig. 22. As the Reynolds number increases, the side force changes along the solid line, and as the Reynolds number decreases, it changes along the dotted line. Therefore, the critical Reynolds number will be different depending on whether Reynolds number (i.e., v) increases or decreases.

Conclusions

1) Flat elliptical forebodies have local directional stability near zero sideslip. The stability region reduces as the incidence is increased.

2) Vertical elliptical forebodies are directionally unstable.

3) Unlike circular forebodies, elliptical forebodies have unique sideslip behaviors and their sideslip behaviors are more predictable.

4) Circular forebodies can have a more significant beneficial contribution to directional stability in comparison to flat elliptical forebodies. Whereas maximum directional instability of circular forebodies are less significant compared to that of vertical elliptic forebodies.

5) It was successfully demonstrated that sideslip behavior can be simply obtained from roll signature data.

6) As a Reynolds number exceeds a critical value, turbulent reattachment starts to occur on one side of the body. The occurrence of reattachment results in an increase in side force at angles of attack greater than 55 deg and a drop in normal force at angles of attack greater than 30 deg.

7) Directional instability for vertical ellipses increases as turbulent reattachment occurs.

8) Hysteresis effects were observed for side force variations near the critical Reynolds number.

References

[1]Chambers, J. R., Anylin, E. L., and Bowman, J. S., "Effects of a Pointed Nose on Spin Characteristics of Fighter Airplane Models Including Correlation with Theoretical Calculations," NASA TN D-5921, Sept. 1970.

[2]Keener, E. R., and Chapman G. T., "Onset of Aerodynamic Side Force at Zero Sideslip on Symmetric Forebodies at High Angles of Attack," AIAA Paper 74-770, Aug. 1974.

[3]Coe, P. L., Jr., Chambers, J. R., and Letko, W., "Asymmetric Lateral-Directional Characteristics of Pointed Bodies of Revolution at High Angles of Attack," NASA TN D-7095, Nov. 1972.

[4]Lamont, P. J., and Kennaugh, A., "Multiple Solutions for Aircraft Sideslip Behaviour at High Angles of Attack," AIAA Paper 89-0645, Jan. 1989.

[5]Lamont, P. J., and Kennaugh, A., "Total Incidence Plane Aerodynamics: The Key to Understanding High Incidence Flight Dynamics," *Journal of Aircraft*, Vol. 28, No. 7, 1991, pp. 431–435.

[6]Grafton, S. B., Groum, M. A., and Nguyen, L. T., "High Angle of Attack Stability Characteristics of Three Surface Fighter Configurations," NASA TM 84584, March 1983.

[7]Brandon, J. M., and Nguyen, L. T., "Experimental Study of Effects of Forebody Geometry on High Angle of Attack Static and Dynamic Stability," AIAA Paper 86-0331, Jan. 1986.